

Time-Graph Frequency Representation with Singular Value Decomposition for Neural Speech Enhancement

Tingting Wang¹, Tianrui Wang², † Meng Ge², Qiquan Zhang³, Zirui Ge¹, Zhen Yang¹

¹Nanjing University of Posts and Telecommunications, Nanjing, China,

²Tianjin Key Laboratory of Cognitive Computing and Application, College of Intelligence and Computing, Tianjin University, Tianjin, China, ³The University of New South Wales, Sydney, Australia.

Abstract—Time-frequency (T-F) domain methods for monaural speech enhancement have benefited from the success of deep learning. Recently, focus has been put on designing two-stream network models to predict amplitude mask and phase separately, or, coupling the amplitude and phase into Cartesian coordinates and constructing real and imaginary pairs. However, most methods suffer from the alignment modeling of amplitude and phase (real and imaginary pairs) in a two-stream network framework, which inevitably incurs performance restrictions. In this paper, we introduce a graph Fourier transform defined with the singular value decomposition (GFT-SVD), resulting in real-valued time-graph representation for neural speech enhancement. This real-valued representation-based GFT-SVD provides an ability to align the modeling of amplitude and phase, leading to avoiding recovering the target speech phase information. Our findings demonstrate the effects of real-valued time-graph representation based on GFT-SVD for neural speech enhancement. The extensive speech enhancement experiments establish that the combination of GFT-SVD and DNN outperforms the combination of GFT with the eigenvector decomposition (GFT-EVD) and magnitude estimation UNet, and outperforms the short-time Fourier transform (STFT) and DNN, regarding objective intelligibility and perceptual quality. We release our source code at: https://github.com/Wangfighting0015/GFT_project.

Index Terms—speech enhancement, graph Fourier transform, spectral mapping, singular value decomposition.

I. INTRODUCTION

Speech enhancement aims to reconstruct the clean speech signal from the noisy speech recording, which often serves as a front-end module for diverse speech applications, such as automatic speech recognition (ASR), speech coding, hearing aids, and speaker recognition [1], [2]. In the past decade, with the flourishing of deep learning technology, speech enhancement has shown great progress, showcasing excellent performance in suppressing highly non-stationary noise sources than traditional statistics-based methods [3]–[6].

Existing neural strategies for speech enhancement mainly utilize either waveform-based [7], [8] or spectrogram-based techniques [9]–[11]. Due to speech and noise patterns tend to be more distinguishable after the short-time Fourier transform (STFT), the spectrogram-based solutions are still the

mainstream solutions, such as UNet [12], DCCRN [13], TF-GridNet [14], and the most recent Mamba-based scheme [15]. Initially, spectrogram-based methods focused on estimating the magnitude only, and reconstructing the waveform using the estimated magnitude and the original noisy phase. This damaged phase directly limits the upper speech quality of the reconstructed waveform. To alleviate the issue, recent studies have moved to the decoupling-style speech enhancement strategy, including magnitude-phase and real-imaginary decoupling methods. The magnitude-phase decoupling methods often employ a dual-stream network architecture to separately reconstruct the magnitude and phase components of the target speech, while the real-imaginary decoupling methods achieve the reconstruction of the target speech’s magnitude and phase indirectly by estimating its real and imaginary components. **Additionally, Lu et al. [16] propose a dual-path speech enhancement model (MP-SENet), which performs parallel denoising of magnitude and phase spectrum.** Thus, the real-imaginary decoupling methods naturally avoid the phase wrapping issue inherent in magnitude-phase decoupling methods, reconstructing the high-fidelity speech signals.

However, such decoupling-style solutions require the exchange of information between the two streams in the designed network to enhance magnitude and phase estimation. This makes it challenging to ensure the information alignment between the two branch networks. For example, Yin et al. [17] observes that when employing the real-imaginary decoupling method (e.g., cIRM [18]) for speech enhancement, the real component is accurately estimated, but the imaginary part is almost zero. In other words, the targets of the two branches (i.e., magnitude and phase) are not equally restored, resulting in misalignment. This potential misalignment issue leads to errors during signal reconstruction, resulting in a degradation of speech quality. Thus, this observation prompts a research question: “How is alignment modeling of magnitude and phase achieved in neural speech enhancement?”.

To answer this question, we first observe that alignment issue arises from the design of dual-stream networks. The key to resolving this issue lies in how to eliminate dual-stream networks while still retaining magnitude and phase information. Motivated by this, we propose the Graph Fourier Transforms (GFTs) using the Singular Value Decomposition

This work was supported by the National Natural Science Foundation of China (Grant 62071242).

† Meng Ge is the corresponding author.

(SVD), called GFT-SVD. The proposed GFT-SVD is capable of projecting raw waveform to a real-valued time-graph representation, rather than the complex-valued representation used in traditional STFT, achieving a near-lossless conversion in the process. This process naturally avoids the requirement for dual-stream network modeling of complex-value representations, and retains both magnitude and phase.

II. PRELIMINARY WORK

A. Graph Representation of Speech Signal

Given a speech frame, the directed graph representation \mathcal{G}_s of speech samples \mathbf{s} in this speech frame is denoted as $\mathcal{G}_s = (\mathcal{V}_s, \mathbf{A}_k)$, where \mathcal{V}_s represents the vertex set and $|\mathcal{V}_s| = N$. $A_k(i, j) = 1$ if the dependency between the i th speech samples residing on vertex v_i and the j th speech samples residing on vertex v_j exists, otherwise $A_k(i, j) = 0$ [19], [20]. k indicates that there is a dependency between a speech sample and neighboring k samples. A graph interpretation of speech graph signals can be achieved by viewing the 0-1 shift matrix as the graph adjacency matrix.

B. Short-Time Fourier Transform vs. Graph Fourier Transform

Given the framed speech signal \mathbf{s} , the Short-Time Fourier Transform (STFT) can convert the time-domain waveform into a complex-valued frequency-domain spectrogram, defined as follows:

$$\mathbf{S} = \text{STFT}(\mathbf{s}) = \mathbf{S}_r + j\mathbf{S}_i \in \mathbb{C}. \quad (1)$$

where \mathbf{S}_r and \mathbf{S}_i are real and imaginary parts of the complex-valued spectrogram of \mathbf{s} .

The Graph Fourier Transform (GFT) is similar to the STFT, consisting of two parts: the Graph Fourier Transform and the inverse Graph Fourier Transform. For example, the Graph Fourier Transform of a signal \mathbf{s} can be denoted as:

$$\mathbf{S}_G = \text{GFT}(\mathbf{s}) = \mathbf{U}^{-1}\mathbf{s} = \mathbf{S}_G^r + j\mathbf{S}_G^i \in \mathbb{C}. \quad (2)$$

Here, \mathbf{U} is the eigenvector matrix of \mathbf{A}_k with the eigenvector decomposition (EVD) method, i.e., $\mathbf{A}_k = \mathbf{U}\mathbf{\Lambda}\mathbf{U}^{-1}$ where $\mathbf{\Lambda}$ is a diagonal matrix of which diagonal elements $\lambda_0, \lambda_2, \dots, \lambda_{N-1}$ denote the graph frequency. Consider that \mathbf{A}_k is not symmetric matrix, the graph Fourier basis \mathbf{U} obtained by the EVD method is a complex eigenvector matrix according to basic matrix decomposition theory. \mathbf{S}_G^r and \mathbf{S}_G^i are the real and imaginary parts of the complex graph spectral of \mathbf{s} . Thus, the inverse Graph Fourier Transform is denoted as

$$\mathbf{s} = \text{iGFT}(\mathbf{S}_G) = \mathbf{U}\mathbf{S}_G. \quad (3)$$

Both STFT and GFT convert waveforms into complex-valued spectrograms, which are challenging to model directly in networks. As a result, decoupling-style network modeling has become a trend, but this strategy also brings the problem of misalignment between the decoupled elements.

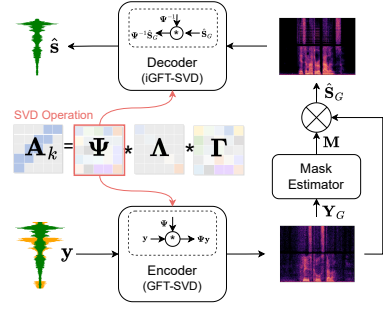


Fig. 1. The overview of our neural speech enhancement with GFT-SVD.

III. METHODOLOGY

The key difference of our proposed approach lies in the encoder and decoder. Unlike the STFT/GFT based encoders and decoders for complex-valued signal transformation, our GFT-SVD leverages Singular Value Decomposition (SVD) to convert signals losslessly into real-valued spectrograms. This approach avoids the misalignment issue caused by decoupling network modeling, thereby minimizing reconstruction losses.

A. Overview

Our proposed approach consists of three parts, including encoder, mask estimator, and decoder, as show in Fig. 1. Both the encoder and decoder utilize the designed real-valued Graph Fourier Transform, specifically GFT-SVD and inverse GFT-SVD (iGFT-SVD), respectively. The mask estimator can be implemented using arbitrary suitable enhancement network.

Formally, given a framed noisy speech \mathbf{y} , after passing through the GFT-SVD encoder, it is transformed into a real-valued spectrogram real-valued time-graph representation \mathbf{Y}_G . Next, the time-graph representation \mathbf{Y}_G is fed into the mask estimator to predict the corresponding masks \mathbf{M} . Finally, the estimated mask is applied to the noisych for denoising, and the clean target speech is reconstructed using the iGFT-SVD. The whole process can be denoted as

$$\mathbf{Y}_G = \text{GFT-SVD}(\mathbf{y}) \in \mathbb{R} \quad (4)$$

$$\hat{\mathbf{S}}_G = \mathbf{M} \odot \mathbf{Y}_G, \hat{\mathbf{s}} = \text{iGFT-SVD}(\hat{\mathbf{S}}_G) \in \mathbb{R}. \quad (5)$$

As seen above, our pipeline operates entirely with real values, avoiding the requirement for traditional dual-branch decoupling structures used to handle complex-valued spectrogram.

B. Real-Valued Graph Fourier Transform

Differing to the graph Fourier basis with EVD, we use singular value decomposition (SVD) method that realizes arbitrary shape matrix decomposition to decompose 0-1 real-valued matrix \mathbf{A}_k , which uses its unitary matrices to define a new graph Fourier basis. That is, $\text{SVD}(\mathbf{A}_k) = \mathbf{\Psi} \times \mathbf{\Lambda} \times \mathbf{\Gamma}$, where the unitary matrix $\mathbf{\Psi}$ and $\mathbf{\Gamma}$ are left and right singular eigen matrix of \mathbf{A}_k , \times represents the multiply operation.

By utilizing the unitary matrix property, $\mathbf{\Psi}$ that consists of real-valued eigen vector can map the noisy speech \mathbf{y} into a real-valued graph frequency domain. Thus, the real-valued Graph Fourier Transform of \mathbf{y} , i.e., Eq. (4), is given by

$$\mathbf{Y}_G = \text{GFT-SVD}(\mathbf{y}) = \mathbf{\Psi}\mathbf{y}. \quad (6)$$

Similarly, the inverse graph Fourier transform of $\hat{\mathbf{S}}_G$ in Eq. (5) can be calculated by the inverse of Ψ , which is denoted as

$$\hat{\mathbf{s}} = \text{iGFT-SVD}(\hat{\mathbf{S}}_G) = \Psi^{-1}\hat{\mathbf{S}}_G. \quad (7)$$

Fig. 2 shows the visualization of real and imaginary parts

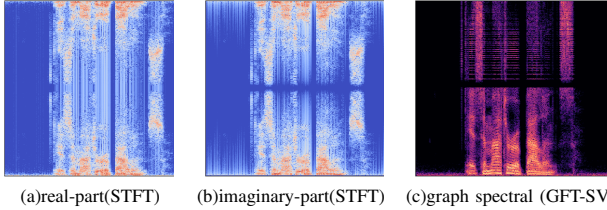


Fig. 2. Example of the clean speech. The real and imaginary parts of clean speech after STFT, and the graph spectral of clean speech after GFT-SVD are visualized for illustration convenience.

of clean speech after STFT and that of the graph spectra of clean speech after GFT-SVD. Observe from Fig. 2, we can see that the real and imaginary parts are symmetrical after STFT extended by traditional symmetrical Fourier series, while the real-valued graph spectra is unsymmetrical and contains amplitude and phase synchronously. It differs from the traditional spectrum with STFT by two steps, which helps the mask trains faithfully better.

C. Mask Estimator and Training Objective

As mentioned earlier, our designed GFT-SVD based encoder and decoder can be adapted to any masking-based enhancement network. Here, we use various networks as mask estimator, including NSnet2 [21], dual-path convolution recurrent network (DPCRN) [22], dense convolutional recurrent network (DCRN) [23], deep complex convolution recurrent network (DCCRN) [13], multi-scale temporal frequency convolutional network with axial self-attention (MTFAA) [24], UNet [12], band-split RNN (BSRNN) [25] and Graph UNet (G-UNet) [26].

The training objective of the entire network is based on the SI-SDR loss [27] between the estimated waveform $\hat{\mathbf{s}}$ and the clean speech \mathbf{s} , which is denoted as follow.

$$\mathcal{L}_{\text{SI-SDR}} = 20 \log_{10} \frac{\|\langle \hat{\mathbf{s}}, \mathbf{s} \rangle\|^2}{\|\hat{\mathbf{s}} - \frac{\langle \hat{\mathbf{s}}, \mathbf{s} \rangle}{\|\mathbf{s}\|^2} \mathbf{s}\|^2}. \quad (8)$$

IV. EXPERIMENTAL RESULTS

A. Dataset and Experimental Setup

We verify the effectiveness of the proposed approach on two benchmark datasets: DNS-2020 and VCTK+DEMAND [28], [29]. The recordings of DNS-2020 dataset are from the 2020 Deep Noise Suppression Challenge, and are sampled at 16 kHz. We generate 100-hour noisy data with SNR ranges from -5dB to 20dB using DNS-2020. The training and validation sets are partitioned from the training data at a ratio of 4:1. VCTK+DEMAND is a simulated dataset. The clean speech is selected from 28 speakers in the Voice Bank corpus [30], while the noisy speech is generated by mixing the clean speech with

TABLE I
PERFORMANCE COMPARISON OF DIFFERENT MODELS BASE ON GFT-SVD WITH \mathbf{A}_3 ON THE NO-REVERB DATASET

Neural Network	Fourier Transform	WB-PESQ	NB-PESQ	SI-SDR (dB)	STOI
NSnet2 [21]	STFT	2.331	2.865	16.262	0.946
NSnet2_G	GFT-SVD	2.439	3.008	16.352	0.950
DPCRN [22]	STFT	2.797	3.260	18.570	0.967
DPCRN_G	GFT-SVD	2.885	3.392	18.964	0.968
DCRN [23]	STFT	2.566	3.074	17.326	0.958
DCRN_G	GFT-SVD	2.739	3.272	18.143	0.962
DCCRN [13]	STFT	2.644	3.148	17.950	0.963
DCCRN_G	GFT-SVD	2.841	3.376	18.587	0.967
MTFAA [24]	STFT	2.696	3.243	18.294	0.964
MTFAA_G	GFT-SVD	2.707	3.261	18.454	0.963
BSRNN [25]	STFT	2.203	2.734	16.070	0.942
BSRNN_G	GFT-SVD	2.321	2.835	16.300	0.943
UNet [12]	STFT	2.017	2.597	14.585	0.940
G-UNet [26]	GFT-EVD	2.580	3.129	17.583	0.959
UNet_G	GFT-SVD	2.785	3.346	18.466	0.966

noise from the Diverse Environments Multichannel Acoustic Noise Database (DEMAND) [31]. The ratio of training to validation utterances in the VCTK+DEMAND dataset is approximately 9:1.

For experimental setup, the window length and hop size are 25 ms and 6.25 ms for all models. The GFT length is 512. 512-dimension graph features are fed into NSnet2, DPCRN, DCRN, DCCRN, MTFAA, UNet, BSRNN and G-UNet networks. Consider that our graph frequency spectrum by GFT-SVD belongs to the real-valued domain, the band merging and splitting process of backbone MTFAA and BSRNN models are removed. NSnet2, DPCRN, DCRN, DCCRN, UNet and G-UNet apply the originally proposed corresponding network. The 512-dimension features after STFT are inputted into the baseline for fairness of comparisons.

Perceptual evaluation of speech quality (PESQ) [32], short-time objective intelligibility (STOI) [33], and scale-invariant signal-to-distortion ratio (SI-SDR) [34] are employed for objective evaluation of enhanced speech signals in the paper.

B. Effectiveness Analysis of GFT-SVD

Table I reports the comparison results of models on the DNS-2020 no-reverb testset, in terms of four metrics. NSnet2_G, DPCRN_G, DCRN_G, DCCRN_G, MTFAA_G, UNet_G and BSRNN_G represent the corresponding backbone network with the GFT-SVD. From Table I, it can be observed that these models of the time-graph representation provide 0.2 gains of average PESQ compared to the backbone networks with STFT and the combination of GFT-EVD and magnitude estimation UNet. In terms of SI-SDR, DPCRN_G, DCRN_G and UNet_G can provide more than 1dB gains over the DPCRN, DCRN, and G-UNet respective.

Table II shows the comparison results of models on the small but commonly-used dataset VCTK+DEMAND. So that we can fairly compare the backbone network based on

TABLE II
PERFORMANCE COMPARISON OF DIFFERENT MODELS BASE ON GFT-SVD WITH \mathbf{A}_3 ON THE VCTK+DEMAND DATASET

Neural Network	Fourier Transform	WB-PESQ	NB-PESQ	SI-SDR (dB)	STOI
NSnet2 [21]	STFT	2.343	3.109	17.793	0.928
NSnet2_G	GFT-SVD	2.462	3.215	18.035	0.932
DPCRn [22]	STFT	2.551	3.333	18.544	0.940
DPCRn_G	GFT-SVD	2.741	3.556	18.826	0.944
DCRN [23]	STFT	2.436	3.211	17.877	0.933
DCRN_G	GFT-SVD	2.624	3.426	18.242	0.937
DCCRN [13]	STFT	2.510	3.255	18.242	0.933
DCCRN_G	GFT-SVD	2.634	3.468	18.125	0.940
MTEAA [24]	STFT	2.657	3.478	18.837	0.938
MTEAA_G	GFT-SVD	2.748	3.553	18.670	0.942
BSRNN [25]	STFT	2.444	3.190	18.831	0.928
BSRNN_G	GFT-SVD	2.567	3.358	19.219	0.932
UNet [12]	STFT	2.160	3.000	16.484	0.926
G-UNet [26]	GFT-EVD	2.455	3.274	18.009	0.932
UNet_G	GFT-SVD	2.644	3.490	18.611	0.937

GFT-SVD with the combination of backbone networks and STFT/GFT-EVD. From Table II, the combination of backbone networks and GFT-SVD has a large gain over the combination of backbone networks like DPCRn, DCRn, and UNet with STFT/GFT-EVD on all the four metrics. This proves the advantage of our time-graph representation based on GFT-SVD for neural speech enhancement.

C. Impact of k Values on GFT-SVD

Fig. 3 shows the influence of GFT-SVD based on \mathbf{A}_k in different cases of k values. Note that k represents the link number of a speech sample with neighbors. We can clearly observe that when k is equal to 3 or 5, the average PESQ and SI-SDR of the combination of GFT-SVD and DNN architectures can rank the best, While the performance of all models will decrease with the increased value of k . This is because GFT-SVD based on \mathbf{A}_k can capture strongly hidden information between neighbor speech sampling points, thus supporting more stable graph spectra of speech signals in the case of the graph frequency domain with $k = 3, 5$.

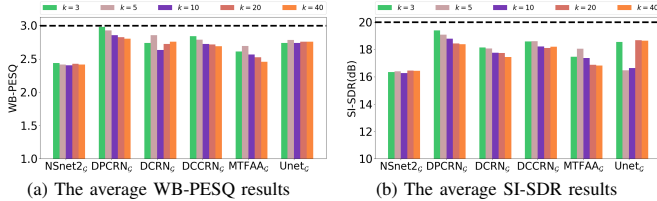


Fig. 3. The average WB-PESQ, SI-SDR of speech enhancement network-based GFT-SVD in different values of k .

D. Evaluation of Computational Efficiency

Table III reports the multiplier-accumulator operations (MACs) and network parameters (#Param). 5 seconds of input audio are used to test the computational cost of the number of MACs per second. The last column results list the real-time factor (RTF) on Nvidia GeForce GTX 3090Ti. Observe from Table III, the combination of GFT-SVD and backbone

TABLE III
THE MACs AND PARAMETERS OF THE COMBINATION OF GFT-SVD AND DIFFERENT MODELS ON NO-REVERB DATASETS

Neural Network	Fourier Transform	MACs (G/s)	#Param (M)	RFT
NSnet2 [21]	STFT	1.91	3.04	0.009
NSnet2_G	GFT-SVD	1.92	3.04	0.006
DPCRn [22]	STFT	62.29	0.88	0.011
DPCRn_G	GFT-SVD	62.49	0.88	0.005
DCRN [23]	STFT	27.54	2.03	0.009
DCRN_G	GFT-SVD	27.63	2.03	0.003
DCCRN [13]	STFT	109.53	4.33	0.031
DCCRN_G	GFT-SVD	109.88	4.33	0.013
MTEAA [24]	STFT	24.22	2.19	0.040
MTEAA_G	GFT-SVD	24.30	2.19	0.012
BSRNN [25]	STFT	3797	200	0.247
BSRNN_G	GFT-SVD	3812	200	0.118
UNet [12]	STFT	37.47	18.10	0.019
G-UNet [26]	GFT-EVD	32.23	18.10	0.025
UNet_G	GFT-SVD	37.47	18.10	0.009

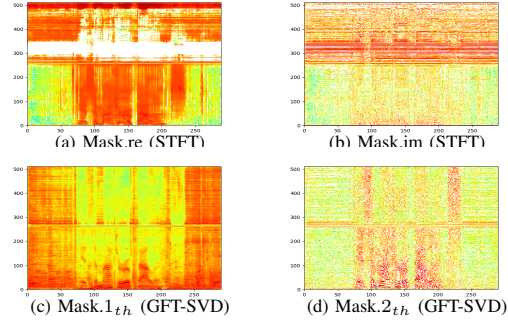


Fig. 4. (a), (b) The real and imaginary parts of the estimated mask in setting DPCRn after STFT. (c), (d) The estimated two stream network mask in setting DPCRn_G after GFT-SVD.

networks performs better than the baseline with the same number of parameters and MACs. These results demonstrated the superiority of GFT-SVD in speech enhancement compared to the combination of STFT/GFT-EVD and backbone networks.

E. Masking Visualization

Fig. 4 confirms the improvement through visualization. Here we visualize the estimated masks in setting DPCRn, DPCRn_G respectively on the VCTK+DEMAND dataset. From the Fig. 4, we can conclude that the real-valued time-graph representation with GFT-SVD contributes to the training mask compared to the traditional complex T-F spectrogram. This time-graph representation significantly improves the phase prediction, helps alignment modeling of amplitude and phase.

V. CONCLUSION

The paper introduces GFT-SVD into neural speech enhancement, which provides a real-valued time-graph representation. It supports an ability of alignment modeling of amplitude and phase in mask-based single-channel speech networks, leading to improving speech quality. Comparison with state-of-the-art systems on both DNS-2020 and VCTK+DEMAND datasets demonstrated the superiority of GFT-SVD over GFT-EVD, STFT on DNN architectures of speech enhancement.

REFERENCES

- [1] P. C. Loizou, *Speech Enhancement: Theory and Practice*, 2nd ed. Boca Raton, FL, USA: CRC Press, Inc., 2013.
- [2] D. Wang and J. Chen, "Supervised speech separation based on deep learning: An overview," *IEEE/ACM Transactions on Audio, Speech, and Language Processing*, vol. 26, no. 10, pp. 1702–1726, 2018.
- [3] M. Krawczyk-Becker and T. Gerkmann, "On MMSE-based estimation of amplitude and complex speech spectral coefficients under phase-uncertainty," *IEEE/ACM Trans. Audio, Speech, and Lang. Proc.*, vol. 24, no. 12, pp. 2251–2262, 2016.
- [4] Y. Ephraim and D. Malah, "Speech Enhancement Using a Minimum Mean-Square Error Short-Time Spectral Amplitude Estimator," *IEEE Trans. Acoust., Speech, Signal Process.*, vol. ASSP-32, no. 6, pp. 1109–1121, 1984.
- [5] Q. Zhang, M. Wang, Y. Lu, L. Zhang, and M. Idrees, "A novel fast nonstationary noise tracking approach based on mmse spectral power estimator," *Digital Signal Processing*, vol. 88, pp. 41–52, 2019.
- [6] Q. Zhang, M. Wang, Y. Lu, M. Idrees, and L. Zhang, "Fast nonstationary noise tracking based on log-spectral power mmse estimator and temporal recursive averaging," *IEEE Access*, vol. 7, pp. 80985–80999, 2019.
- [7] A. Defossez, G. Synnaeve, and Y. Adi, "Real time speech enhancement in the waveform domain," in *Proc. INTERSPEECH*, 2020.
- [8] M. Kolbæk, Z.-H. Tan, S. H. Jensen, and J. Jensen, "On loss functions for supervised monaural time-domain speech enhancement," *IEEE/ACM Trans. Audio, speech, Lang. Process.*, vol. 28, pp. 825–838, 2020.
- [9] Q. Zhang, A. Nicolson, M. Wang, K. K. Paliwal, and C. Wang, "DeepMMSE: A deep learning approach to mmse-based noise power spectral density estimation," *IEEE/ACM Transactions on Audio, Speech, and Language Processing*, vol. 28, pp. 1404–1415, 2020.
- [10] K. Wilson, M. Chinen, J. Thorpe, B. Patton, J. Hershey, R. A. Saurous, J. Skoglund, and R. F. Lyon, "Exploring tradeoffs in models for low-latency speech enhancement," in *Proc. IWAENC*, 2018, pp. 366–370.
- [11] Y. Xu, J. Du, L.-R. Dai, and C.-H. Lee, "A regression approach to speech enhancement based on deep neural networks," *IEEE/ACM Trans. Audio, Speech, and Lang. Proc.*, vol. 23, no. 1, pp. 7–19, 2014.
- [12] O. Ronneberger, P. Fischer, and T. Brox, "U-net: Convolutional networks for biomedical image segmentation," in *Medical Image Computing and Computer Assisted Intervention*, vol. 9351, 2015, pp. 234–241.
- [13] Y. Hu, Y. Liu, and Lv, "Dccrn: Deep complex convolution recurrent network for phase-aware speech enhancement," *Proc. INTERSPEECH*, pp. 2472–2476, 2020.
- [14] Z.-Q. Wang, S. Cornell, S. Choi, Y. Lee, B.-Y. Kim, and S. Watanabe, "Tf-gridnet: Making time-frequency domain models great again for monaural speaker separation," in *ICASSP 2023-2023 IEEE International Conference on Acoustics, Speech and Signal Processing (ICASSP)*, 2023, pp. 1–5.
- [15] X. Zhang, Q. Zhang, H. Liu, T. Xiao, X. Qian, B. Ahmed, E. Ambikairajah, H. Li, and J. Epps, "Mamba in speech: Towards an alternative to self-attention," *arXiv preprint arXiv:2405.12609*, 2024.
- [16] Y. Lu, Y. Ai, and Z. Ling, "Mp-senet: A speech enhancement model with parallel denoising of magnitude and phase spectra," in *Proc. Interspeech*, N. Harte, J. Carson-Berndsen, and G. Jones, Eds., 2023, pp. 3834–3838.
- [17] D. Yin, C. Luo, Z. Xiong, and W. Zeng, "PHASEN: A phase-and-harmonics-aware speech enhancement network," in *The Thirty-Fourth AAAI Conference on Artificial Intelligence*, 2020. AAAI Press, 2020, pp. 9458–9465.
- [18] D. S. Williamson, Y. Wang, and D. Wang, "Complex ratio masking for monaural speech separation," *IEEE/ACM Trans. Audio, Speech, and Lang. Proc.*, vol. 24, no. 3, pp. 483–492, 2015.
- [19] A. Ortega, P. Frossard, J. Kovacevic, J. M. F. Moura, and P. Vandergheynst, "Graph signal processing: overview, challenges, and applications," *Proc. IEEE*, vol. 106, no. 5, pp. 808–828, 2018.
- [20] T. Wang, H. Guo, X. Yan, and Z. Yang, "Speech signal processing on graphs: the graph frequency analysis and an improved graph wiener filtering method," *Speech Commun.*, vol. 127, pp. 82–91, 2021.
- [21] Y. Xia, S. Braun, C. K. A. Reddy, H. Dubey, R. Cutler, and I. Tashev, "Weighted speech distortion losses for neural-network-based real-time speech enhancement," in *Proc. IEEE Int. Conf. Acoust., Speech, Signal Process.*, 2020, pp. 871–875.
- [22] X. Le, H. Chen, K. Chen, and J. Lu, "DPCRN: dual-path convolution recurrent network for single channel speech enhancement," *CoRR*, vol. abs/2107.05429, 2021. [Online]. Available: <https://arxiv.org/abs/2107.05429>
- [23] A. Pandey, C. Liu, Y. Wang, and Y. Saraf, "Dual application of speech enhancement for automatic speech recognition," in *IEEE Spoken Language Technology Workshop*, 2021, pp. 223–228.
- [24] G. Zhang, C. Wang, L. Yu, and J. Wei, "Multi-scale temporal frequency convolutional network with axial attention for multi-channel speech enhancement," in *Proc. IEEE Int. Conf. Acoust., Speech, Signal Process.*, 2022, pp. 9206–9210.
- [25] Y. L. Jianwei Yu, Hangting Chen, "High fidelity speech enhancement with band-split rnn," 2024. [Online]. Available: <https://arxiv.org/pdf/2212.00406>
- [26] C. Zhang and X. Pan, "Single-channel speech enhancement using graph fourier transform," in *Proc. INTERSPEECH*, 2022, pp. 946–950.
- [27] T. Wang, Z. Pan, M. Ge, Z. Yang, and H. Li, "Time-domain speech separation networks with graph encoding auxiliary," *IEEE Signal Process. Lett.*, vol. 30, pp. 110–114, 2023.
- [28] S. Lv, Y. Hu, S. Zhang, and L. Xie, "DCCRN+: channel-wise subband DCCRN with SNR estimation for speech enhancement," in *Proc. INTERSPEECH*, 2021, pp. 2816–2820.
- [29] C. K. A. Reddy, V. Gopal, R. Cutler, E. Beyrami, R. Cheng, H. Dubey, S. Matusevych, R. Aichner, A. Aazami, S. Braun, P. Rana, S. Srinivasan, and J. Gehrke, "The INTERSPEECH 2020 deep noise suppression challenge: Datasets, subjective testing framework, and challenge results," in *Proc. INTERSPEECH*, 2020, pp. 2492–2496.
- [30] C. Veaux, J. Yamagishi, and S. King, "The voice bank corpus: Design, collection and data analysis of a large regional accent speech database," in *Proc. Int. Conf. Oriental COCOSDA, Nov 2013*, 2013, pp. 1–4.
- [31] J. Thiemann, N. Ito, and E. Vincent, "The diverse environments multichannel acoustic noise database: A database of multichannel environmental noise recordings," in *Acoust. Soc. Am.*, vol. 133, no. 5, 2013, p. 3591–3591.
- [32] A. W. Rix, J. G. Beerends, M. P. Hollier, and A. P. Hekstra, "Perceptual evaluation of speech quality (pesq)-a new method for speech quality assessment of telephone networks and codecs," in *Proc. IEEE Int. Conf. Acoust., Speech, Signal Process.*, 2001, pp. 749–752.
- [33] C. H. Taal, R. C. Hendriks, R. Heusdens, and J. Jensen, "A short-time objective intelligibility measure for time-frequency weighted noisy speech," in *Proc. IEEE Int. Conf. Acoust., Speech, Signal Process.*, 2010, pp. 4214–4217.
- [34] J. L. Roux, S. Wisdom, H. Erdogan, and J. R. Hershey, "SDR - half-baked or well done?" in *Proc. IEEE Int. Conf. Acoust., Speech, Signal Process.*, 2019, pp. 626–630.